Naval Research Laboratory

Washington, DC 20375-5000 NRL Memorandum Report 5832 July 31, 1986

Numerical Simulations of the Flowfield in a Central-Dump Ramjet Combustor

I. Tests of the Model and Effects of Forcing

K. KAILASANATH, J. GARDNER, J. BORIS AND ELAINE ORAN

Laboratory for Computational Physics

This work was sponsored by the Office of Naval Research and the Naval Air Systems Command.

SECURITY CLASSIFICATION OF THIS PAGE

AD-A170 936

REPORT DOCUMENTATION PAGE

1a REPORT SECURITY CLASSIFICATION: UNCLASSIFIED	1b RESTRICTIVE MARKINGS
2a SECURITY CLASSIFICATION AUTHORITY	3 DISTRIBUTION/AVAILABILITY OF REPORT: Approved for public release; distribution unlimited.
2b DECLASSIFICATION/DOWNGRADING SCHEDULE	
4 PERFORMING ORGANIZATION REPORT NUMBER(S): NRL Memorandum Report 5832	5 MONITORING ORGANIZATION REPORT NUMBER(S)
6a NAME OF PERFORMING ORGANIZATION: Naval Research Laboratory; 6b OFFICE SYMBOL (If applicable): Code 4040	7a NAME OF MONITORING ORGANIZATION
6c ADDRESS (City, State, and ZIP Code): Washington, DC 20375-5000	7b ADDRESS (City, State, and ZIP Code)
8a NAME OF FUNDING/SPONSORING ORGANIZATION: Office of Naval Research; 8b OFFICE SYMBOL (If applicable)	9 PROCUREMENT INSTRUMENT IDENTIFICATION NUMBER
8c ADDRESS (City, State, and ZIP Code): Arlington, VA 22217	10 SOURCE OF FUNDING NUMBERS: PROGRAM ELEMENT NO. 61153N; PROJECT NO; TASK NO RR024-03-01; WORK UNIT ACCESSION NO. DN480-664

11 TITLE (Include Security Classification): Numerical Simulations of the Flowfield in a Central-Dump Ramjet Combustor
I. Tests of the Model and Effects of Forcing

12 PERSONAL AUTHOR(S): Kailasanath, K., Gardner, J., Boris, J. and Oran, Elaine

13a TYPE OF REPORT	13b TIME COVERED	14. DATE OF REPORT (Year, Month, Day)	15 PAGE COUNT
Interim	FROM ____ TO ____	1986 July 31	36

16 SUPPLEMENTARY NOTATION
This work was sponsored by the Office of Naval Research and the Naval Air Systems Command.

17. COSATI CODES		
FIELD	GROUP	SUB-GROUP

18. SUBJECT TERMS (Continue on reverse if necessary and identify by block number)
Numerical simulations Central-dump Ramjet combustor
Flowfield

19 ABSTRACT (Continue on reverse if necessary and identify by block number)

In this paper we presents results of numerical simulations of the cold flow in a central-dump ramjet combustor. ~~We present tests of the boundary conditions and numerical resolutions used to perform the simulations. We then use the simulations to isolate and study the interaction between acoustic waves and large scale vortex structures.~~ A strong coupling between the acoustic modes of the chamber and large scale vortex structures is observed. The results in the early part of the calculations indicate unforced natural vortex growth near the entrance to the combustor (dump plane) at a frequency close to that of the first longitudinal acoustic mode. With time, the acoustic modes shift the frequency of the most amplified vortex-rollup mode near the dump plane into resonance with the acoustic mode. The simulations indicate that the location in space where the modes grow can also be shifted by acoustic forcing. An interesting feature observed in the simulations is a low frequency mode corresponding to the arrival of the merged vortex structures at the choked exit. This mode causes major changes in the merging pattern of the vortices.

20 DISTRIBUTION/AVAILABILITY OF ABSTRACT ☐ UNCLASSIFIED/UNLIMITED ☐ SAME AS RPT ☐ DTIC USERS	21. ABSTRACT SECURITY CLASSIFICATION
22a NAME OF RESPONSIBLE INDIVIDUAL	22b TELEPHONE (Include Area Code) / 22c. OFFICE SYMBOL

DD FORM 1473, 84 MAR — 83 APR edition may be used until exhausted. All other editions are obsolete.

SECURITY CLASSIFICATION OF THIS PAGE

CONTENTS

NUMERICAL SIMULATIONS OF THE FLOWFIELD IN A CENTRAL-DUMP RAMJET COMBUSTOR

I. Tests of the Model and Effects of Forcing

INTRODUCTION

Detailed numerical modelling of the interactions among the various physical and chemical processes which take place within a ramjet combustor is difficult because of the large differences in the important length and time scales involved. This has led to the development of zonal modelling techniques in which various regions of the ramjet combustor are modelled seperately, and the results are then coupled to provide an overall description of the flowfield[1-3]. These models are not truly predictive since they are heavily dependent on a priori knowledge of the flowfield. However, by careful adaptation of the parameters used in such models, successful comparisons to experimental data can be achieved[3]. More recently, numerical simulations have been used to study the flowfield in both axisymmetric centerbody[4] and dump combustors[5-7]. In the numerical study of a dump-combustor flowfield[5] fair agreement was observed between the computed quantities, such as mean axial velocity profiles, and experimental data. Furthermore, the computations gave a steady solution with a large recirculation zone. However, the simulations of a centerbody combustor[5] showed an oscillating flowfield with periodic vortex shedding. Both of these simulations did not consider the effects of an exit nozzle or acoustic forcing on the flowfield in the combustor. More recent simulations have considered the effects of exit nozzles[6,7] and the effects of acoustic forcing[6]. In an earlier work[6] we used numerical simulations to study the effects of acoustic waves on the flowfield in an axisymmetric dump combustor with a choked flow through the exit nozzle. Our results not only showed the periodic shedding of vortices but also the presence of a low frequency mode related to the interaction of vortices with the exit nozzle. In this report we present a more detailed description of the work presented at the JANNAF combustion meeting[6].

Manuscript approved May 23, 1986

A schematic of the idealized central-dump ramjet combustor used in the simulations is shown in Figure 1. The size of the chamber and the mean flow characteristics were chosen to model the experiments presented by Schadow et al.[8]. A cylindrical jet with a mean velocity of 50 m/s flows into a cylindrical dump with twice the jet diameter. The length of the dump, which acts as an acoustic cavity, is varied to change the first longitudinal mode frequency. An exit nozzle at the end of the chamber is accurately modelled to produce choked flow.

In this paper we first discuss the numerical simulation model and present tests of the numerical resolution and boundary conditions. We then discuss two calculations performed on a non-uniform 40×100 grid in detail. In the first we did not impose any acoustic forcing on the system, while in the second we excited the first longitudinal acoustic mode of the chamber with an external acoustic source. We then use these simulations to discuss the effects of forcing. Finally we compare the results of the simulations to experimental observations.

THE NUMERICAL MODEL

The numerical model used to perform the simulations solves the time-dependent conservation equations for mass, momentum and energy in two spatial dimensions. The algorithm used for convective transport is the Flux-Corrected Transport (FCT) algorithm[9] configured in axisymmetric geometry. This is a conservative, monotonic algorithm with fourth-order phase accuracy. FCT algorithms are constructed as a weighted average of a low-order and a high-order finite difference scheme. During a convective transport timestep, FCT first modifies the linear properties of the high-order algorithm by adding low-order diffusion. This prevents dispersive ripples from appearing, and it ensures that all conserved quantities remain suitably monotonic and positive. FCT then subtracts out the added diffusion in regions away from discontinuities. Thus it maintains a high-order of accuracy where it is meaningful while enforcing positivity and monotonicity where it is necessary. With various initial and boundary conditions, this algorithm has been used previously to solve a wide variety of problems in subsonic and supersonic flows.

The calculations presented below are inviscid, that is, no explicit term representing physical viscosity has been included in the model. Also, no artificial viscosity is needed to stabilize the algorithm. There is a residual high order numerical diffusion present which effectively behaves like a viscosity term for short wavelength modes on the order of the zone size. Unlike most numerical methods, however, FCT damping of the short wavelength modes is nonlinear. Thus the effects of this residual viscosity diminish very quickly (much faster than k^2) for the long wavelength modes, which results in a high "effective Reynolds number". The effect of the numerical viscosity on the flow instability frequencies is discussed later. In the problem considered in this paper, we are primarily interested in the interaction of the acoustic modes with large scale vortex structures, which is essentially an inviscid interaction.

For the calculations presented in this paper, the computational cell spacing was set up initially and held fixed in time. Fine zones were used near the entrance to the combustor (the dump plane) in both the radial and axial directions. In both directions the cell sizes gradually increased away from the dump plane. For the calculations presented here using a 40×100 grid, the cell sizes in the axial direction decreased from 8.53 cm at the inlet plane to 0.42 cm at the dump plane, and then gradually increased to 0.50 cm at the rear wall of the combustor (the exit plane). In the radial direction, cell sizes increased from 0.15 cm at

the step to 0.167 cm at both the axis and the outer wall of the combustor. The effects of numerical resolution were checked by comparing two-dimensional calculations with 20 × 50, 40 × 100 and 80 × 200 cells. These grids were generated by either doubling or halving the cell sizes used in the 40 × 100 grid. The timesteps were chosen to satisfy the Courant condition.

Boundary Conditions

The initial thrust of our modelling program has been to develop appropriate inflow and outflow boundary conditions. The outflow conditions force the flow to become sonic at the throat of the exit nozzle. At the solid walls the normal fluxes are set to zero and we extrapolate the pressure to the normal stagnation condition. Since viscosity is not explicitly included in the calculations, no condition is imposed on the tangential velocity at the walls. At the inflow, the pressure is allowed to fluctuate, but we specify the mass flow rate and the inflow velocity and its direction is taken to be axial. These conditions allow acoustic waves to reflect without amplification or damping at the inflow. As a test of the inflow boundary conditions we imposed a planar acoustic source at the rear boundary and observed the pressure fluctuations in the mouth of the inlet. As seen in Figure 2, the pressure at a particular position in the mouth of the inlet varies with a constant amplitude and frequency which corresponds to that of the forcing function. As further test of the boundary conditions, we note that the average flow properties in the combustion chamber calculated using the numerical model agree with those measured in the experiments[8].

RESULTS AND DISCUSSION

The physical dimensions of the inlet and combustor used in the calculations are given in Figure 1. In addition, the exit consists of an annular ring at 0.69 D (from the axis of the combustor) with an area of 8.69 cm^2. The mass inflow rate is 0.38 kg/s with a mean velocity of 50 m/s. The initial chamber pressure is 186 kPa. These conditions were chosen to match those in the experiments of Schadow et al.[8].

The numerical simulations predict values of the density, momentum and energy for each of the computational cells as a function of time. From this information we can selectively generate the data required for various diagnostics. In the analysis presented below, we use two diagnostics extensively; the fourier analysis of pressure fluctuations at various positions in the dump chamber, and instantaneous flow visualization at selected time intervals. For flow visualization, we primarily use streamline contours, although density and vorticity contours are also used. We have also used information gained by studying velocity fluctuations to corroborate the observations based on the pressure fluctuations.

Calculations with and without acoustic forcing were performed. For the calculations with forcing, the first longitudinal acoustic mode was excited at various amplitudes by imposing a time-dependent source of pressure and acoustic energy at the rear wall of the chamber. The source is nearly planar since the entire area inside the annular exit was forced. In all the calculations presented here, the frequency of the source is 446 Hz, which corresponds to the first longitudinal acoustic mode of the dump chamber. Below we first discuss tests of the numerical resolution and then compare calculations with and without acoustic forcing.

Tests of Numerical Resolution

The grid size required to resolve the important features of the flowfield was determined by comparing calculations with three different grids: 20 × 50, 40 × 100 and 80 × 200. The instantaneous flowfields observed with the three different resolutions are shown in Figures 3 and 4. Figure 3 shows the early stages in the evolution of the flowfields and Figure 4 shows the flowfields at a later time. In these figures, the quantities are shown as if the computational grids were evenly spaced. That is, the quantities are plotted at each grid point rather than at their actual physical positions. Thus the figures are not drawn to scale. Figure 1 shows the actual physical dimensions of the system modelled and later in this paper we show the flowfield in true scale. We have found that displaying the results as

we have done in Figures 3 and 4 helps to bring out the similarities and differences between the calculations using the three different grids.

In Figure 3, the 40 × 100 and 80 × 200 grids show two large scale vortical structures and the beginnings of a third one near the dump plane. However, the 20 × 50 grid does not show the formation of the third vortex. In Figure 4, the 20 × 50 shows only three vortices while the other two grids show five vortices. In general, we conclude that the large scale structures are essentially the same with the 40 × 100 and 80 × 200 grids and the 20 × 50 grid is too coarse to resolve the finer scale structures resolved by the other two calculations. Furthermore, as shown in Figure 5, the solution on the 20 × 50 grid eventually settles down to a steady solution with a large recirculation zone. The solutions with the finer grids show a quasi-steady periodic flowfield with vortex shedding and merging. The 40 × 100 grid appears to be adequate to resolve the instantaneous flowfield.

We note that when the grid size is changed, both the resolving capability of the grid and the thickness of the initial shear layer at the dump plane change. Thus the good agreement observed between the instantaneous flowfields at a particular time does not imply that all the shear layer instability frequencies are the same with different resolutions. With the finer 80 × 200 grid, smaller structures and higher frequencies can be resolved than with the coarser (40 × 100) grid. However, the dominant features of the periodic flowfield are essentially the same with the two resolutions. This can be seen in Figures 6 and 7 where the density and streamline contours are compared at two different times after the calculations show a periodic flowfield.

In Figure 6, the flowfields are shown at about 44.78 ms. The agreement between the calculations with the two grids is good. Both calculations show a small vortical structure near the dump plane , a large one near the exit plane and a couple of vortices in between. In Figure 7, the flowfields are shown at about 49.15 ms, which is 4000 timesteps later than the flowfields in Figure 6 with the 40 × 100 grid. The flowfields shown in the two figures are during the same cycle because as shown later, the entire flowfield repeats with a period of 6000 timesteps with the 40 × 100 grid. In Figure 7, the vortical structure seen earlier near the exit plane in Figure 6 has partially exited and a new small vortical structure is seen near the dump plane. We also see three vortices in between the two mentioned above. The good agreement observed between the calculations with the two grids gives us some confidence in using the 40 × 100 grid to study the acoustic-vortex interactions. Later on we also show that the dominant frequencies seen near the dump plane are essentially the same with the two grid resolutions.

Calculations without Forcing

We first discuss an unforced calculation on a 40 × 100 grid. The calculations were run for a long time (60,000 timesteps) and flow visualization showed that an essentially periodic solution was attained. The pressure fluctuations at a number of axial and radial positions have been calculated and fourier analysed. These include positions at the wall, in the shear layer, and along the axis of the combustor. Figure 8 shows the frequency spectrum at 0.1 D and 0.5 D downstream from the dump plane in the shear layer. At both of these positions, we observe a large amplitude at about 144 Hz. Below we show that this frequency corresponds to the time between successive vortices arriving at the rear wall of the combustor. Therefore 144 Hz appears to be related to the interaction of a large vortex structure with the exit nozzle. This interaction is discussed in more detail below.

Besides 144 Hz , we do not see any other dominant frequency at 0.1 D. However we also note the presence of some fluctuations at frequencies between 3000 and 3500 Hz. These may be associated with transverse acoustic modes of the chamber. At 0.5 D, in addition to 144 Hz, we also see significant amplitudes at about 440 Hz and 880 Hz. Since the 440 Hz peak is highly localized, it seems to be a characteristic frequency of the shear layer at this position. The fourier analysis of the velocity fluctuations at the same two locations, 0.1 D and 0.5 D, are shown in Figure 9. These also show that the fluctuations at 144 Hz are significant at both locations, but the fluctuations at 440 Hz are significantly larger at 0.5 D than at 0.1 D. Flow visualization shows the appearance of vortex structures near 0.5 D at a frequency of about 440 Hz. Therefore we conclude that 440 Hz corresponds to pressure and velocity fluctuations associated with vortex structures generated by the most amplified frequency at this position in the shear layer.

Fourier analysis of pressure fluctuations at the corresponding two axial positions at the wall and the axis of the combustor show much smaller amplitudes near 446 Hz, which corresponds to the frequency of the first longitudinal acoustic mode. The appearance of this frequency at these positions indicates that even in unforced calculations, there is some modulation of pressure waves by the natural acoustic properties of the chamber.

The effect of the acoustics of the chamber can also be seen by comparing the fourier analysis of the pressure fluctuations in the shear layer during the early stages (timesteps 5000 to 15,000) of the evolution of the flow to those at later times. In Figure 10, the most amplified frequency at 0.5 D is 405 Hz. However, after the flow goes through a number of cycles and the acoustic mode has built up, this frequency shifts to 440 Hz, as seen earlier in

Figure 8. This shift in frequency implies that the acoustics of the chamber play a definite role even in cases which are not externally forced.

Calculations with Acoustic Forcing

We also performed calculations in which we imposed an acoustic perturbation. Here we consider the case in which the imposed amplitude was 0.5% of the initial chamber pressure, and the frequency of the perturbation was 446 Hz. All other parameters of the calculation were the same as in the unforced case described above. The pressure fluctuations were fourier analyzed at the same two axial positions in the shear layer as they were in the unforced case and the results are shown in Figure 11. At 0.5 D, the amplitude corresponding to 446 Hz has significantly increased from the unforced value. We also see higher harmonics of the 446 Hz peak, as well as the low frequency peak at 144 Hz discussed earlier. The amplitude corresponding to 446 Hz is even higher at 0.1 D. Since the amplitude at 446 Hz for the unforced case was very weak at 0.1 D, we conclude that forcing has not only increased the amplitude of the fluctuations, but has also shifted the location of the shear layer instability (corresponding to 446 Hz) slightly further upstream.

The RMS velocity fluctuations at 0.1 D, for both the forced and the unforced case, are shown in Figure 12 as a function of the radial distance from the axis of the combustor. We note that the fluctuation level in the region where the vortices are forming ($R > 0.5$ D) is significantly larger in the forced case than in the unforced case. This corroborates the observation made above that forcing has shifted the location where the 446 Hz begins to grow to further upstream. This should also result in a larger momentum thickness in the forced case at 0.1 D. This is indeed found to be the case as shown in Figure 13, which shows the momentum thickness as a function of position for both the forced and the unforced case. The momentum thickness is a measure of the shear layer growth for positions within 2 to 3 D from the dump plane. For larger distances from the dump plane, it is a questionable measure since the vortical structures have grown to a size where they interact with the wall.

Figure 13 shows that the momentum thickness for the forced case is larger than for the unforced case. However, for distances greater than about 0.6 D the difference between the two cases is small. To verify this observation, we have compared the RMS velocity fluctuations at 1.12 D for the two cases in Figure 14. The fluctuation levels are seen to be about the same with and without forcing. So the effects of acoustic forcing is concentrated in the positions close to the dump plane.

In an earlier section of this paper it was mentioned that the dominant frequencies near the dump plane are essentially the same with the 40 × 100 and 80 × 200 grids. The fourier analysis of the pressure fluctuations in the shear layer at a position 0.45 D downstream from the dump plane is shown in Figure 15. The data used to obtain this figure is from a calculation on a 80 × 200 grid. This figure should be compared to Figure 11 which is for a calculation on a 40 × 100 grid. Comparing the two figures we see that the dominant frequencies and relative amplitudes are essentially the same.

Evolution of the Flowfield

Streamline contours of the instantaneous flowfield provide a useful visual diagnostic for studying the structure of the flow. Although the streamline contours show the direction of the flow at a particular instant, the magnitude of the flow velocity is not well represented. Hence the shape of the vortex structures are well defined while their strengths are not. As an example, consider Figure 16, which shows the density and vorticity contours along with the streamline contours at a particular time (33.86 ms, step 31,000). By this time, the flow has undergone a number of cycles and has settled down to a quasi-steady periodic behavior. The vorticity contours show clumps of vorticity centered at about 0.4 D, 1.3 D, 2.6 D and 5.2 D. These correspond to the vortical flowfield seen in the streamline contours. The density contours show the typical behavior seen in shear flows. Comparing the contours shows the relation between the variations in density, the vorticity contours and the streamline contours.

Further evidence that forcing at the locally most amplified frequency produces highly periodic and coherent vortex structures can be seen from studying streamline contours of the instantaneous flowfield. Figure 17 shows the streamline contours within the dump chamber at a sequence of times. The various frames in this figure are instantaneous "snapshots" of the flowfield taken 1.093 ms apart. This corresponds to 1000 timesteps in the calculation. The timestep corresponding to each of the frames in the figure is indicated on the left of the frame. In each frame, the dump plane is at the left and the exit plane is at the right. The paths of the various vortices are also indicated in the figure. In the first frame (timestep 31000) we see a vortex structure near the dump plane. In the second frame (timestep 32000) this structure has grown and moved downstream. In the third frame (timestep 33000) not only has this structure moved further downstream, but a new structure has formed near the dump plane. This process continues with a new, large-scale vortex structure appearing near the dump plane at intervals of approximately

2000 timesteps. Thus in the figure we clearly see new large scale structures appearing near the dump plane at timesteps 33000, 35000, 37000, 39000, 41000 and 43000. This corresponds to a frequency of 458 Hz, in close agreement with the fourier analysis of the pressure fluctuations which gave a frequency of 446 Hz. The small disagreement of 8 Hz is an artifact of showing the flowfield snapshots at intervals of 1000 timesteps rather than 1017 timesteps.

In Figure 17, we also see that the structures which were first seen near the dump plane at timesteps 31000 and 33000 have merged (paired) at about 2.4 D by timestep 37000. As this large, merged structure moves downstream, a new vortex which was first seen near the dump plane at timestep 35000 merges with it. This new merging occurs by timestep 43000 at about 4.8 D. The structures which appeared near the dump plane at timesteps 37000 and 39000 merge together at about 2.4 D by timestep 43000. That is, at either 2.4 D or 4.8 D, a merging is observed only at about every 6000 timesteps which corresponds to a frequency of about 150 Hz. Since new vortices appear near the dump plane every 2000 timesteps, we note that two successively generated vortices do not always merge with each other.

The time evolution of the flowfield described above correlates well with the fourier analysis of the pressure and velocity fluctuations observed at various axial locations in the combustor. In Figure 18 we show the fourier analysis of the pressure fluctuations at the axial locations, 1.0, 3.0, 4.0 and 5.1 D . All the locations are at the level of the step, a constant radial distance of 0.5 D from the axis of the combustor. At 1.0 D, 446 Hz is the dominant frequency and this corresponds to the passage frequency of the vortices first seen near the dump plane. This location is similar to 0.5 D since no new major events occur between these two locations. At 3.0 D, we see a very large amplitude at 144 Hz. The amplitude of this frequency has increased from what we saw at 1.0 D because of the vortex mergings that occur between 1.0 D and 3.0 D. In Figure 17 we noticed that mergings occured near 2.4 D at a frequency of 144 Hz. At 3.0 D, we also see a new feature in the spectrum, there is significant amplitude corresponding to 300 Hz. As discussed earlier, two successively generated vortices do not always merge with each other at 2.4 D. Therefore, at 3.0 D not only does a merged large vortex pass by, but also a smaller vortex which will eventually merge with the larger one near 4.8 D. Then, as expected, at 4.0 D we see all three frequencies. At 5.1 D, the amplitude at 144 Hz has increased again because of the mergings which take place near 4.8 D at that frequency. Furthermore we no longer see significant amplitude at 300 Hz because only one type of large merged vortex will pass by

5.1 D. At all the locations we see some amplitude corresponding to the forcing frequency of 446 Hz and the low frequency of 144 Hz.

Figure 17 shows that the entire flow undergoes a complete cycle approximately every 6000 timesteps. For example at timesteps 33,000 and 39,000 a large-scale structure has partially exited through the nozzle. At these times, we also see the same number of structures of about the same sizes at about the same positions in the chamber. This similarity exists between any two frames which are 6000 timesteps apart. The frequency corresponding to this cycle is about 150 Hz, which is close to the value of 144 Hz observed in all of the pressure analyses. This also shows that the large-scale flow has settled down to an essentially periodic behavior.

Before this periodic behavior is established, a different kind of merging pattern is observed. In the early stages of the calculation, we observed successively generated vortex structures merging with each other. This results in a vortex merging at 2.4 D every 4000 steps, as shown in Figure 19. The merging frequency estimated from the figure is 229 Hz, which is a subharmonic of the most energetic frequency at the dump plane. This frequency is also close in value to 215 Hz, which was identified by Schadow et al.[8] as the most energetic frequency at about 2 D.

Once the first vortex begins to exit through the nozzle, this periodicity of the vortex merging is lost and the new periodicity corresponding to about 6000 time steps (about 144 Hz) is observed. This frequency is the same frequency as that observed in the fourier analysis of pressure fluctuations throughout the chamber all the way from the dump plane to the exit nozzle. This seems to indicate that an acoustic pulse is generated by vortices exiting the combustor. This pulse then travels upstream to the dump plane and thus provides a feedback mechanism that sustains the oscillations. The odd pairing of the vortices discussed earlier is an important element in the feedback loop since it results in the vortices reaching the exit plane at a frequency of 144 Hz. This phenomenon is very similar to that observed by Ho and Nosseir[10] in their study of the dynamics of a jet impinging on a flat plate. They observed a low frequency oscillation whose period depended on the convective speed of the coherent structures, the speed of the upstream-propagating waves, and the distance between the jet nozzle and the plate.

SUMMARY AND CONCLUSIONS

The results of the calculations presented in this paper indicate a strong coupling between the acoustic modes of the chamber and large-scale vortex structures. In the early stages of the calculations, there is an unforced natural vortex growth near the dump plane at a frequency of 405 Hz. This frequency is close but not equal to the first longitudinal acoustic mode frequency, which is about 446 Hz. As the calculation evolves with time the acoustic modes of the chamber interact with the natural vortex growth so the frequency of the most amplified mode near the dump plane shifts into resonance with the acoustic mode. This is in general agreement with the experimental observations of Schadow et al.[8] in an essentially identical system. They observed that in all their acoustically forced experiments, the most amplified frequency near the dump plane was 460 Hz, and the most amplified frequency in a free jet with a similar configuration was 411 Hz. The numerical simulations also indicate that the location in space where the modes grow can also be shifted by acoustic forcing.

An interesting feature seen in these calculations and first reported at the JANNAF meeting[6] is the low frequency mode corresponding to the arrival of the vortex structures at the choked exit. This mode causes major changes in the merging pattern of the vortices, such as the odd pairing of the vortices. Such a low-frequency mode has also been observed in other two-dimensional numerical simulations[7]. However, this low frequency mode is not observed in the experimental results reported by Schadow et al.[8]. This feature of the flow may be less prominent if three-dimensional instabilites break up the large-scale vortices sufficiently before they reach the exit plane. In addition, this feature may also have been amplified in the calculations by the localized annular nature of the exit boundary. The size of the dump chamber and the mean inflow velocity also play a role because the passage time of the vortices from the dump plane to the exit is affected by these parameters. These possibilites and the general properties of this low-frequency mode are currently under investigation.

ACKNOWLEDGMENTS

This work was sponsored by the Office of Naval Research and the Naval Air Systems Command. The authors would like to thank Drs. Klaus Schadow and William Clarke for their many helpful discussions.

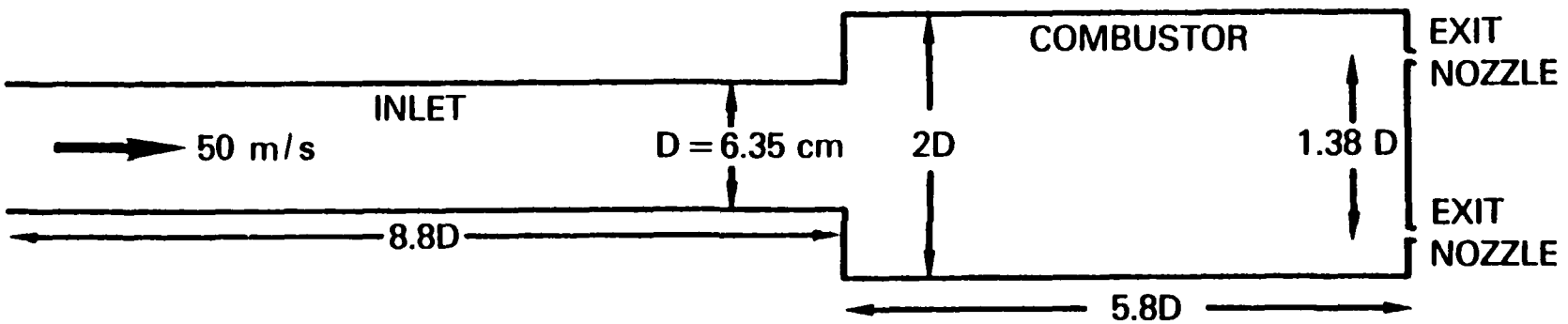

Figure 1. Configuration of idealized axisymmetric ramjet combustor.

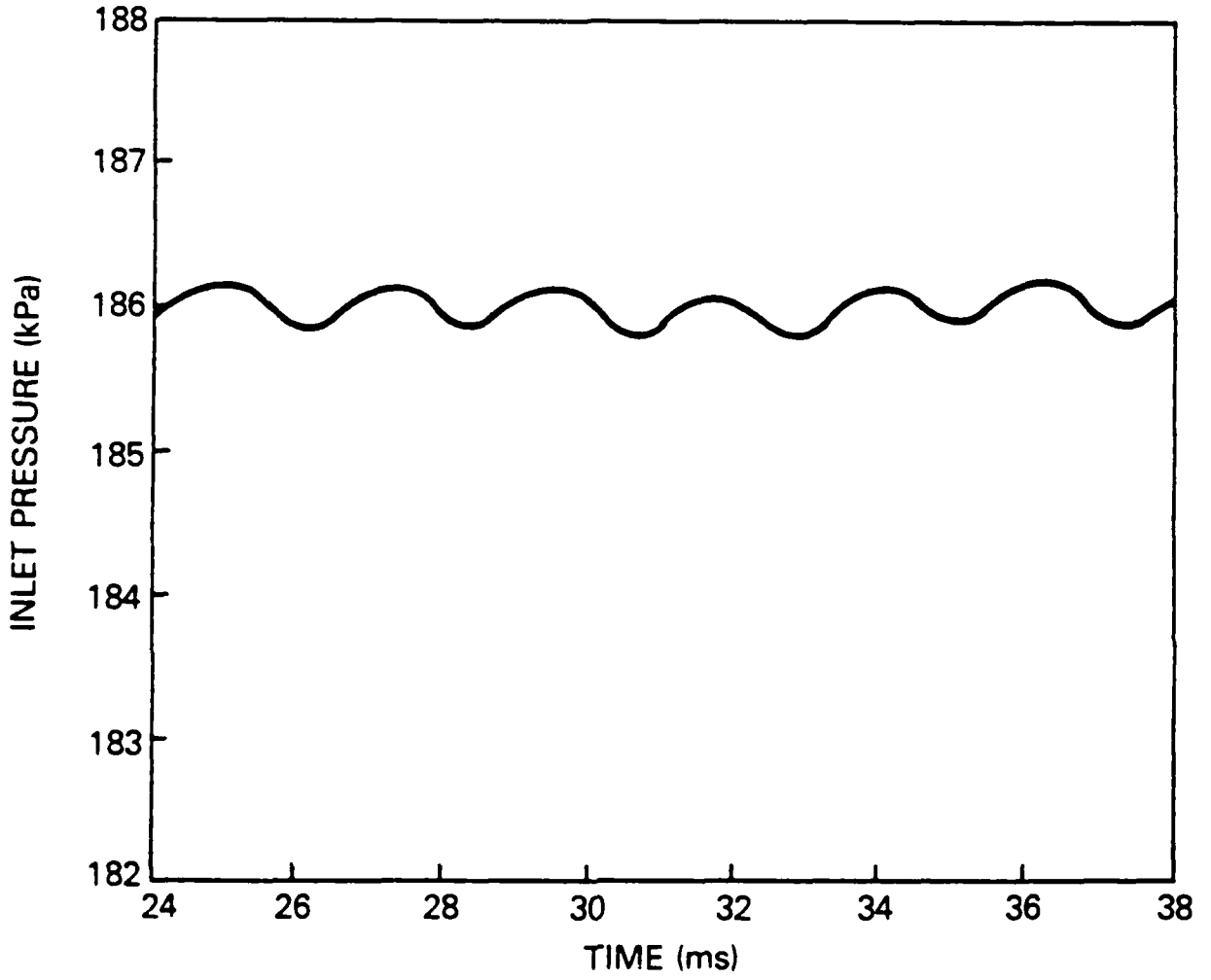

Figure 2. Pressure fluctuations at one position in the mouth of the inlet as a function of time.

STREAMLINES

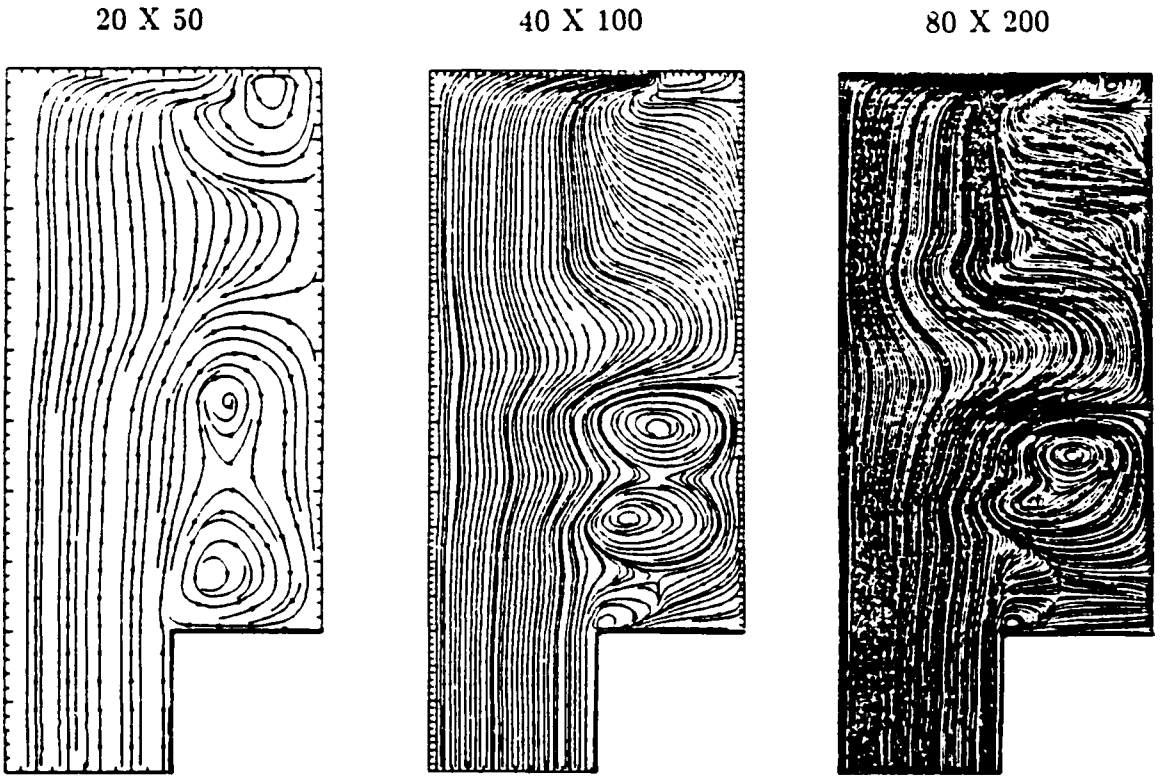

Figure 3. Comparison of streamline contours from the early stages of calculations using 20 × 50 grid, 40 × 100 grid, and 80 × 200 grid. Note that these figures are not drawn to scale. The actual dimensions of the system modelled are shown in Figure 1.

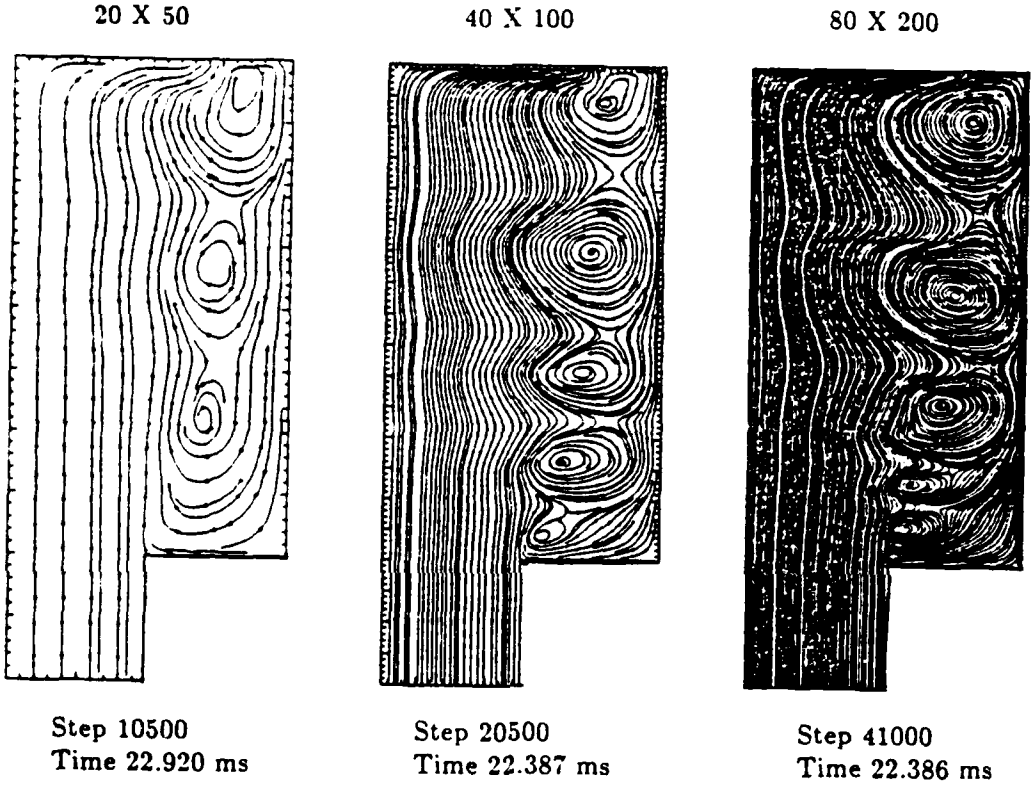

Figure 4. Comparison of streamline contours from the later stages of calculations using 20×50 grid, 40×100 grid, and 80×200 grid. Note that these figures are not drawn to scale. The actual dimensions of the system modelled are shown in Figure 1.

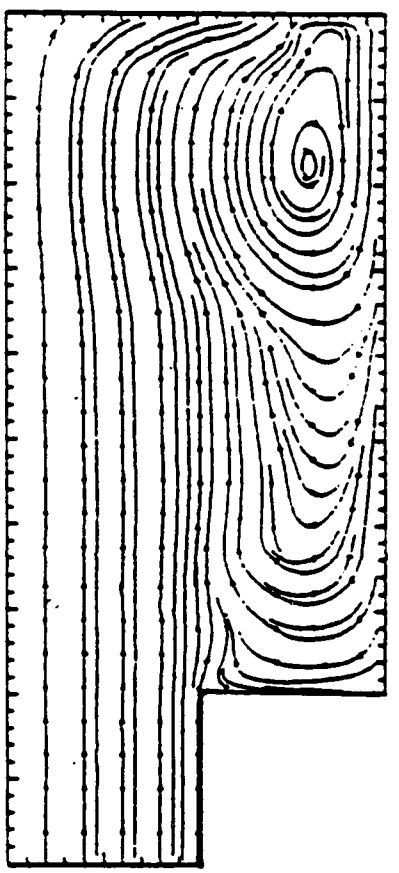

Figure 5. The streamline contours showing the steady solution obtained for a calculation without forcing using a 20 × 50 grid.

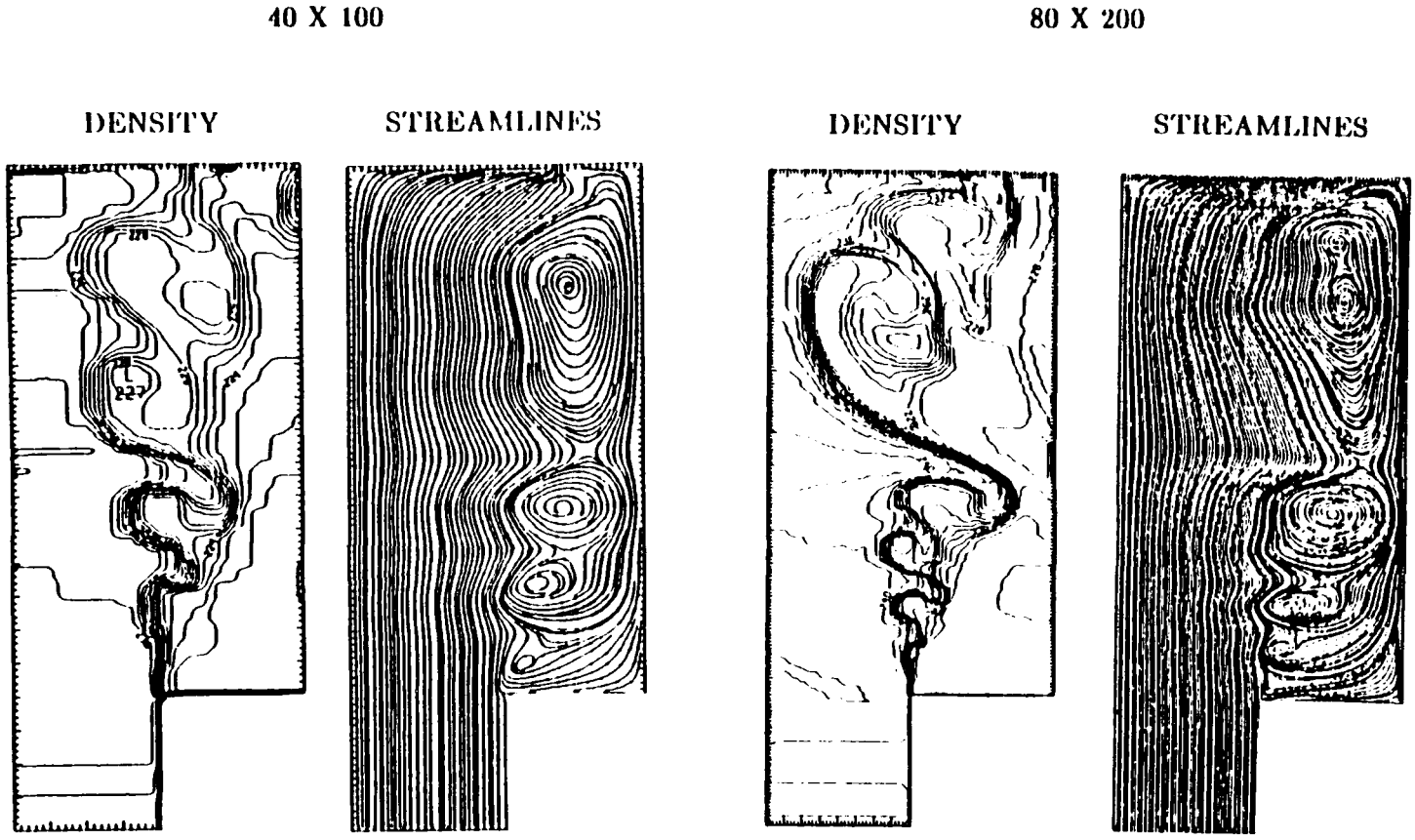

Figure 6. Comparison of density and streamline contours from calculations using a 40 × 100 and a 80 × 200 grid. Note that these figures are not drawn to scale. The actual dimensions of the system modelled are shown in Figure 1.

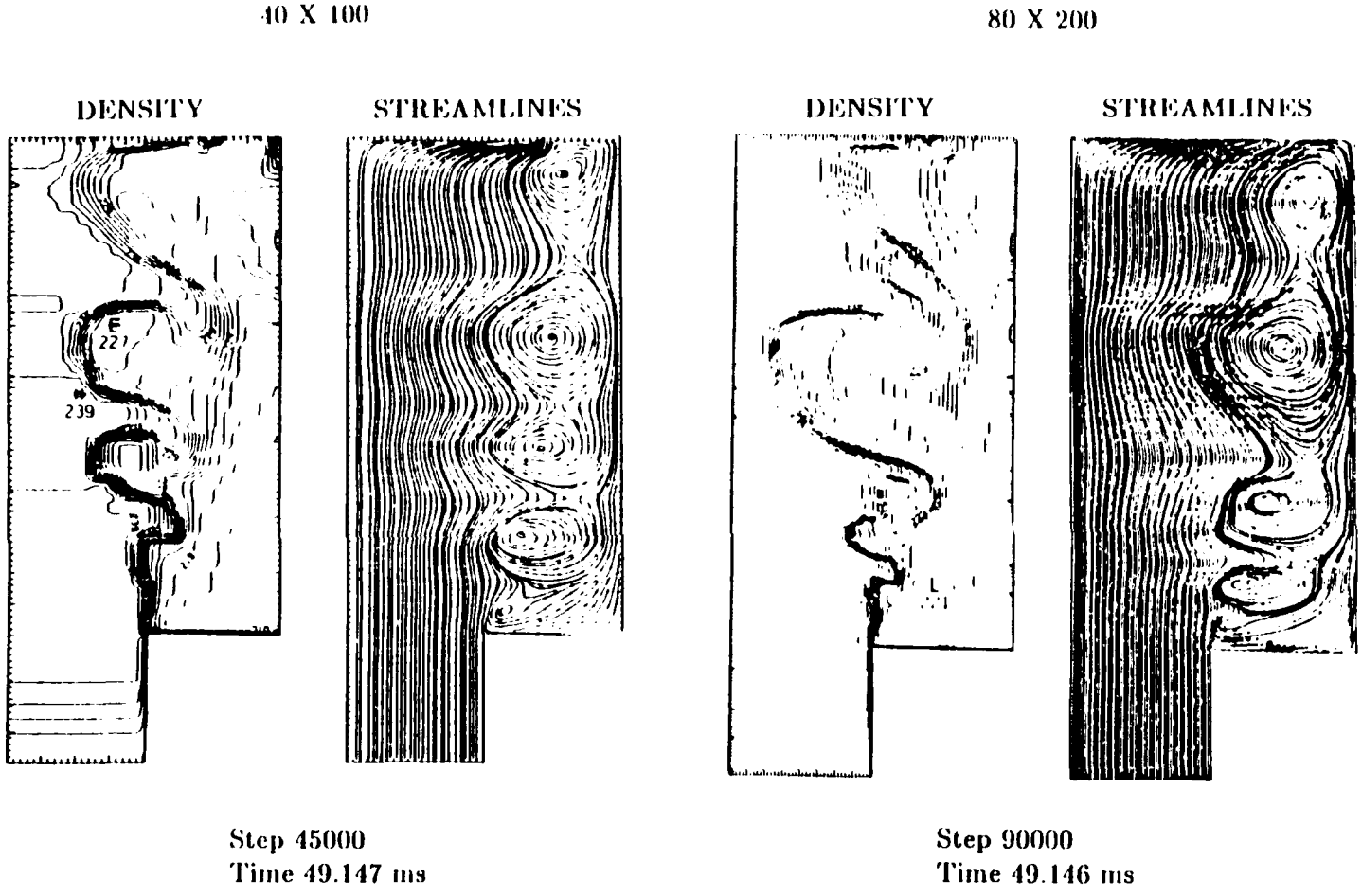

Figure 7. Further comparison of density and streamline contours from calculations using a 40 × 100 and a 80 × 200 grid. Note that these figures are not drawn to scale. The actual dimensions of the system modelled are shown in Figure 1.

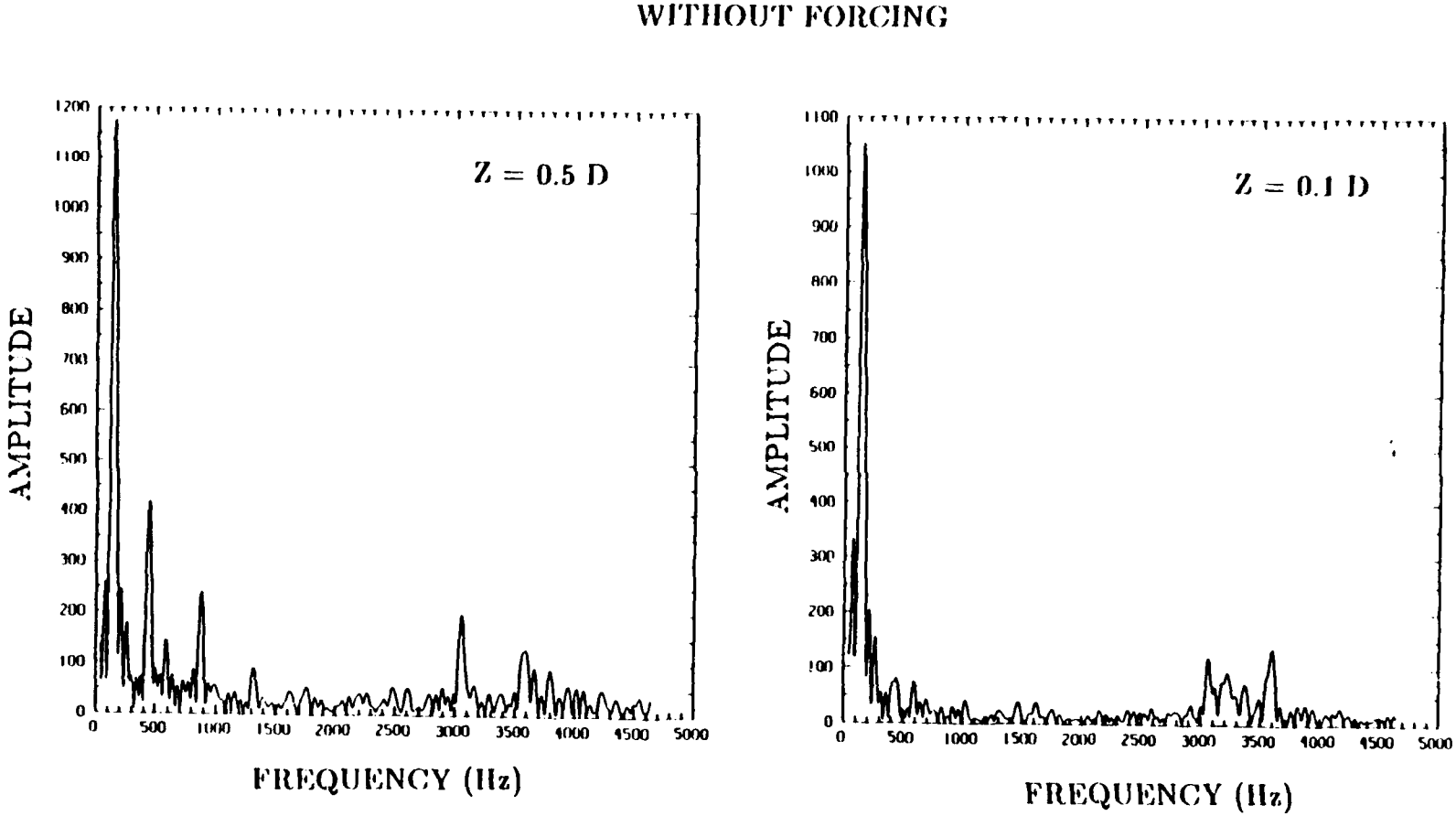

Figure 8. The frequency spectrum of pressure fluctuations at two positions in the shear layer from the later stages of a calculation without forcing. The two positions are 0.1 D and 0.5 D downstream from the dump plane.

WITHOUT FORCING

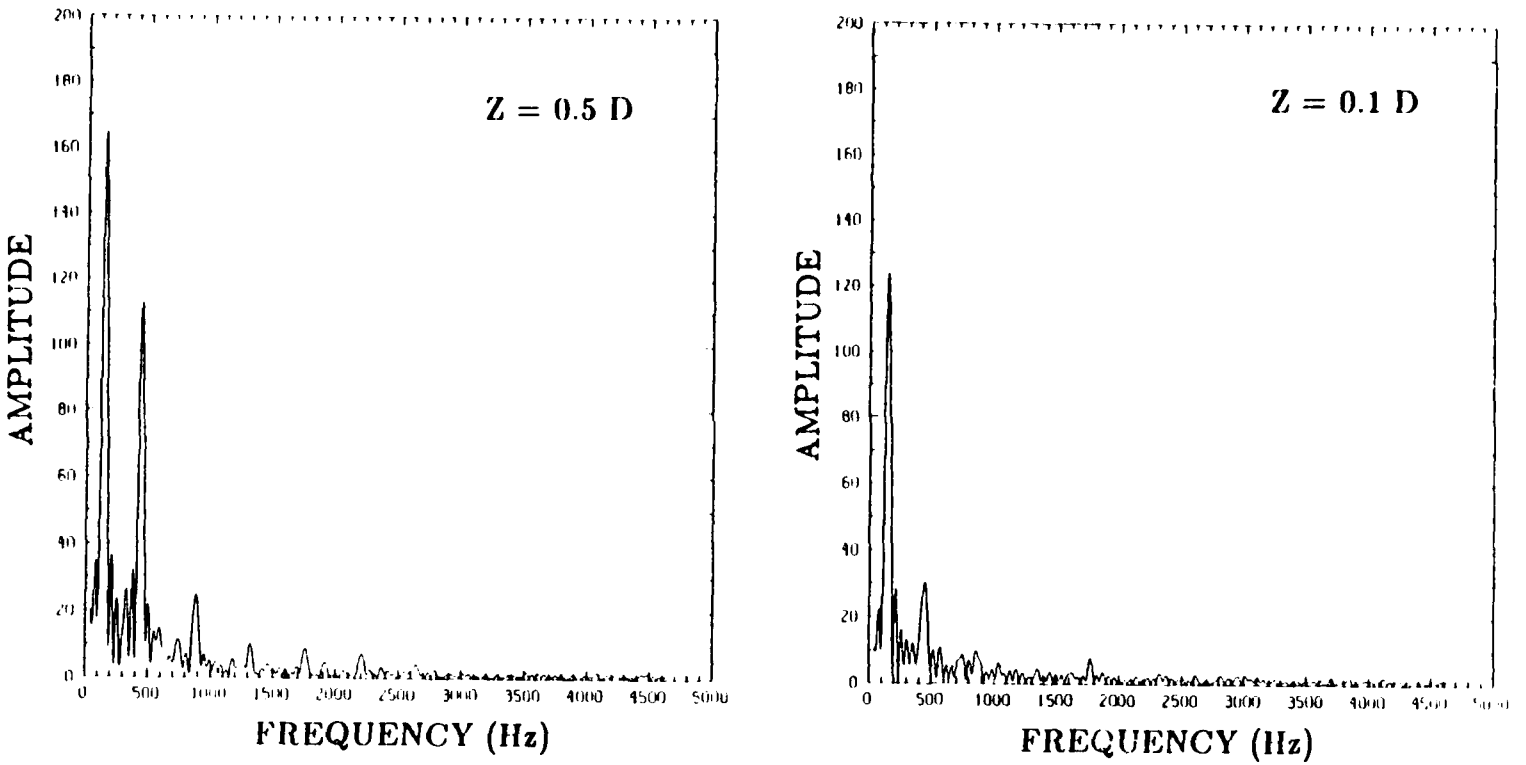

Figure 9. The frequency spectrum of velocity fluctuations at the same two positions in the shear layer as in Figure 8.

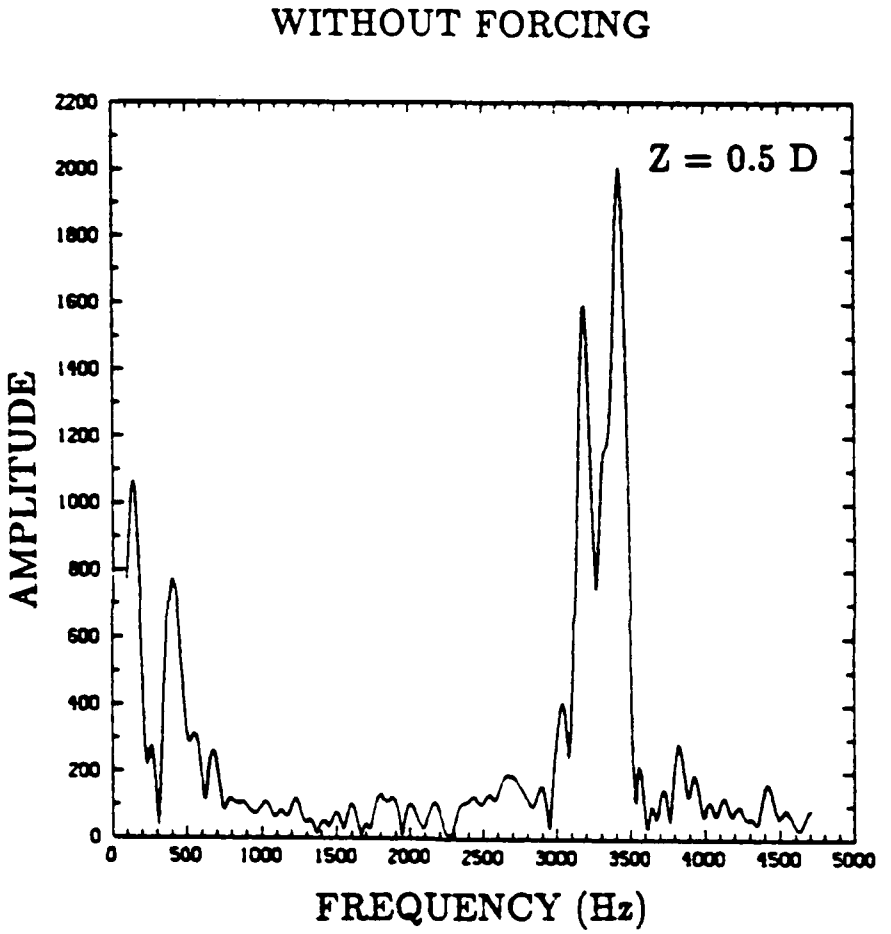

Figure 10. The frequency spectrum of pressure fluctuations in the shear layer at 0.5 D during the early stages of the calculation without forcing.

WITH FORCING

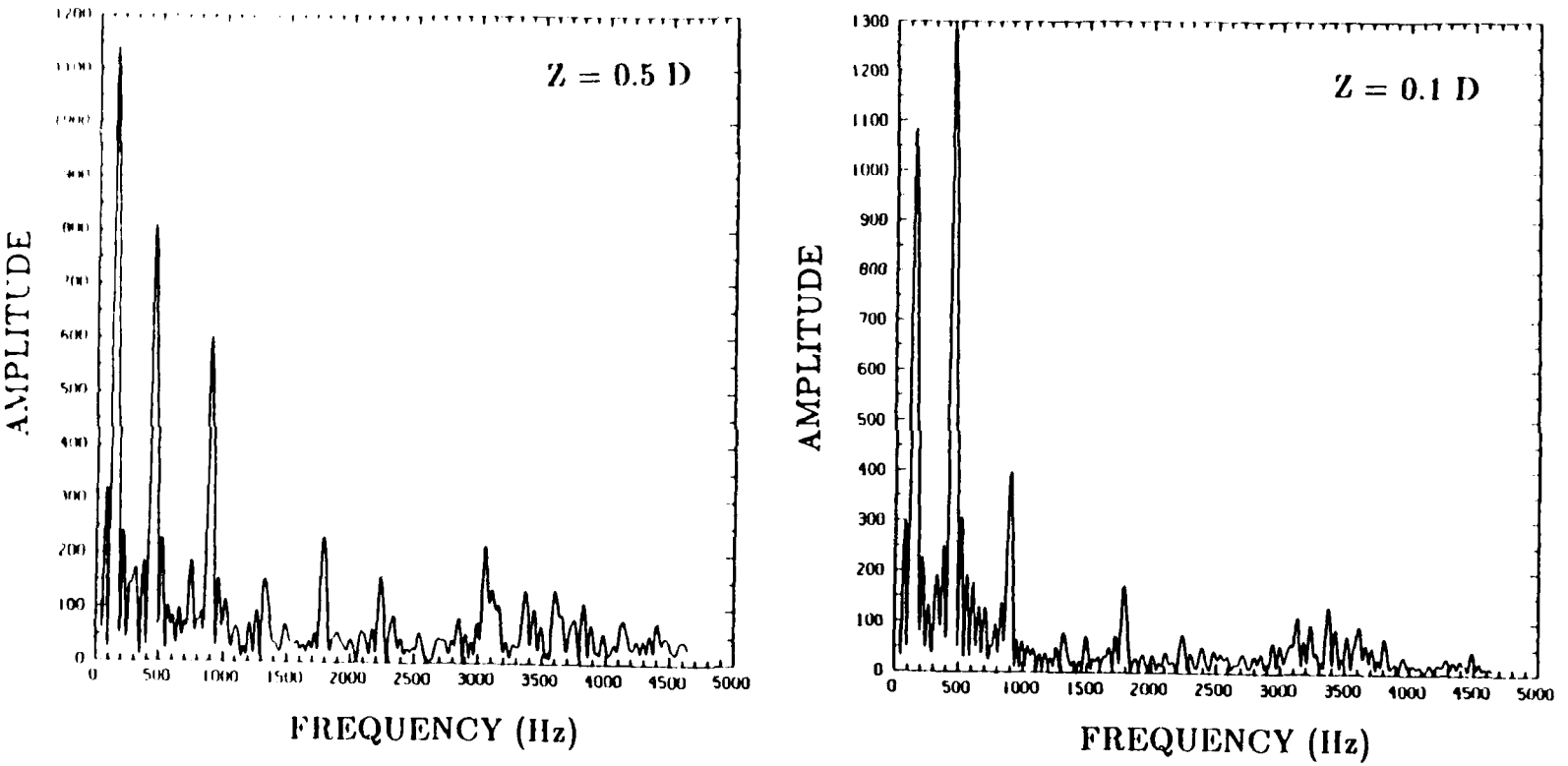

Figure 11. The frequency spectrum of pressure fluctuations at two positions in the shear layer from the later stages of a calculation with acoustic forcing. The forcing amplitude was 0.5% of the initial chamber pressure and the frequency was 446 Hz.

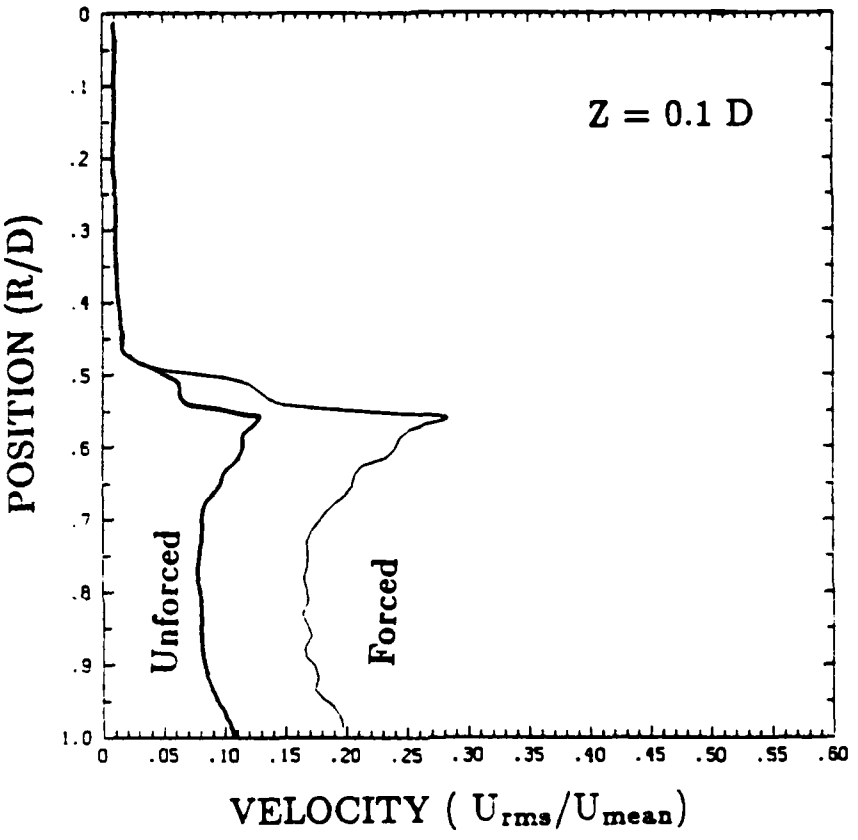

Figure 12. Comparison of the profiles of the RMS velocity fluctuations at 0.1 D from calculations with and without acoustic forcing. For the forced case, the forcing amplitude was 0.5% of the initial chamber pressure and the frequency was 446 Hz.

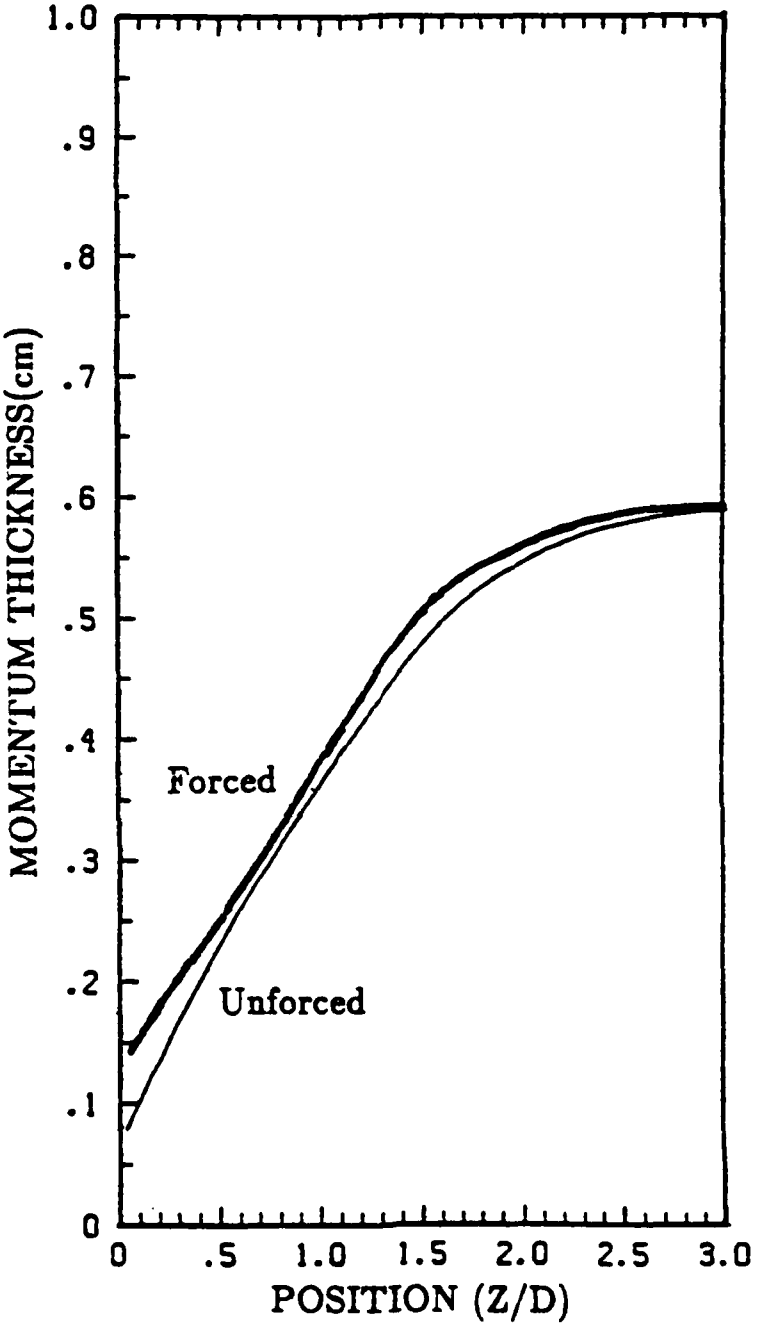

Figure 13. Comparison of growth of momentum thickness from calculations with and without acoustic forcing. For the forced case, the forcing amplitude was 0.5% of the initial chamber pressure and the frequency was 446 Hz.

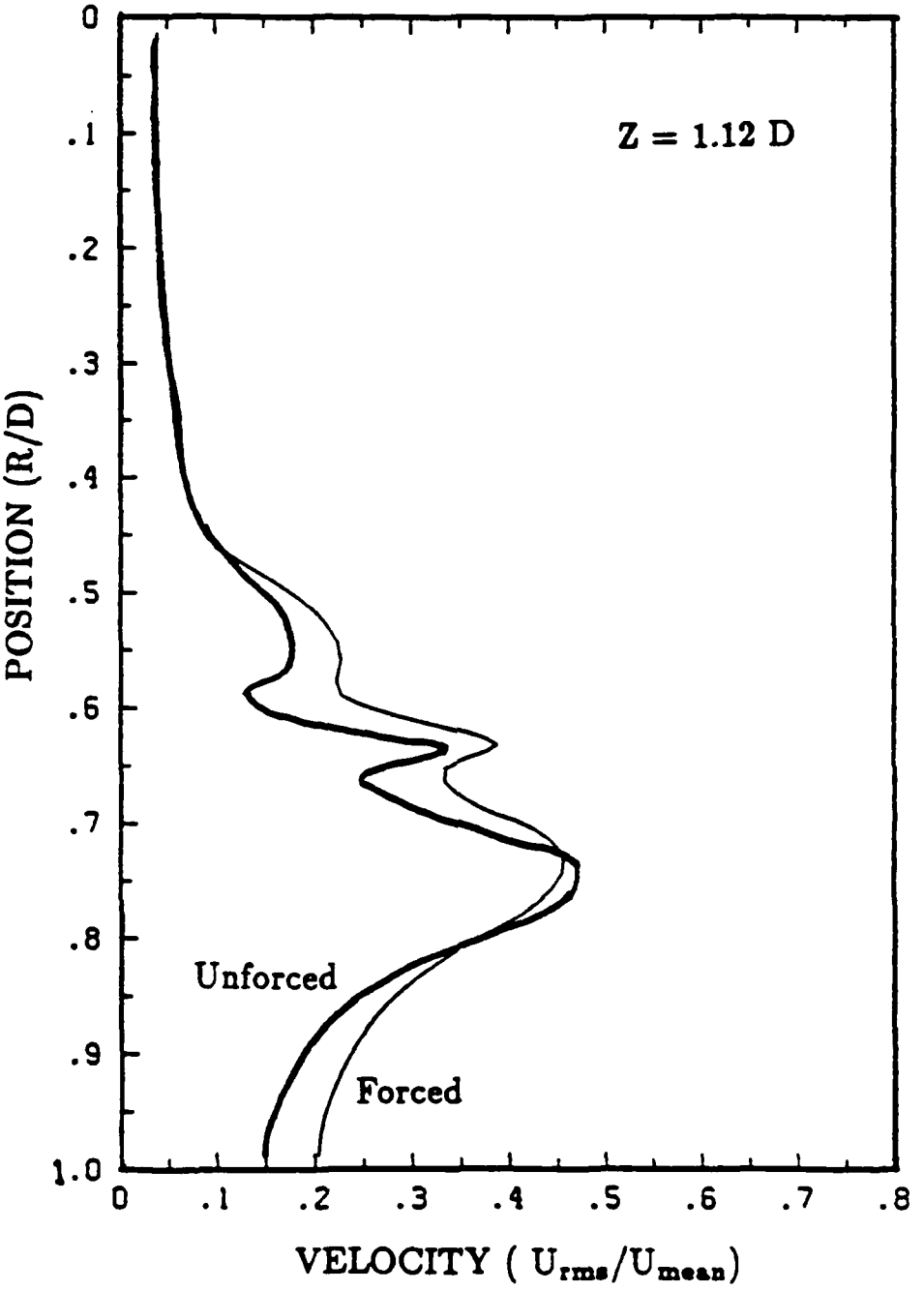

Figure 14. Comparison of the profiles of the RMS velocity fluctuations at 1.12 D from calculations with and without acoustic forcing. For the forced case, the forcing amplitude was 0.5% of the initial chamber pressure and the frequency was 446 Hz.

WITH FORCING

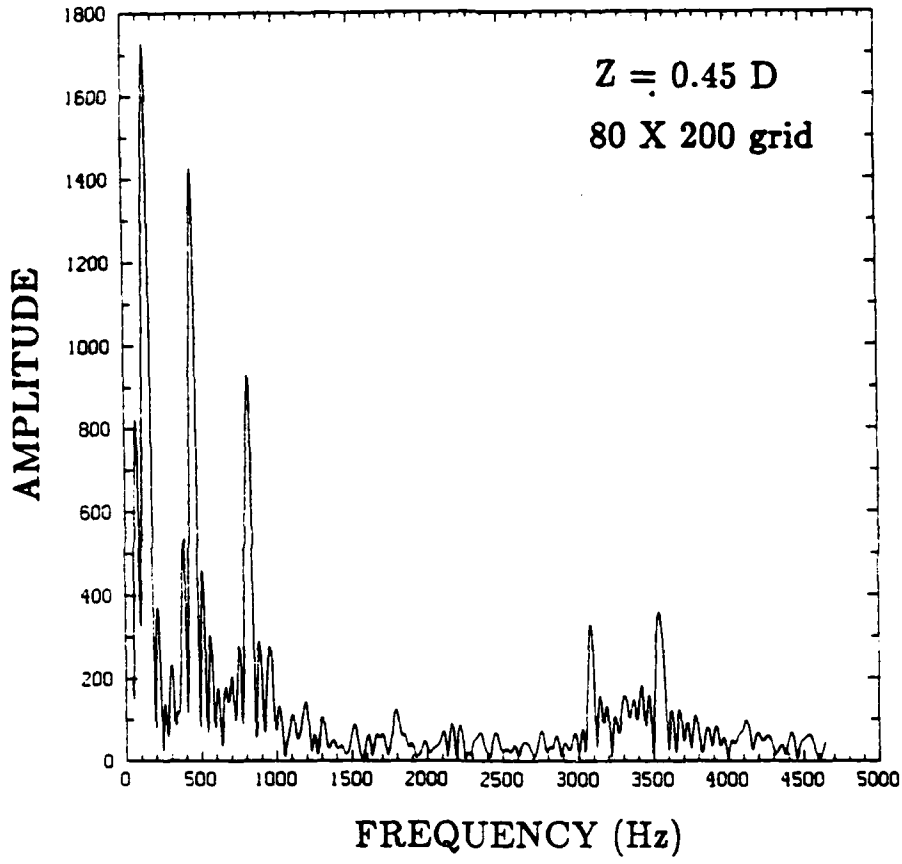

Figure 15. Effect of numerical resolution on the frequency spectrum of pressure fluctuations at 0.45 D in the shear layer from the later stages of a calculation with forcing. The forcing amplitude was 0.5% of the initial chamber pressure and the frequency was 450 Hz.

Step 31000
Time 33.86 ms

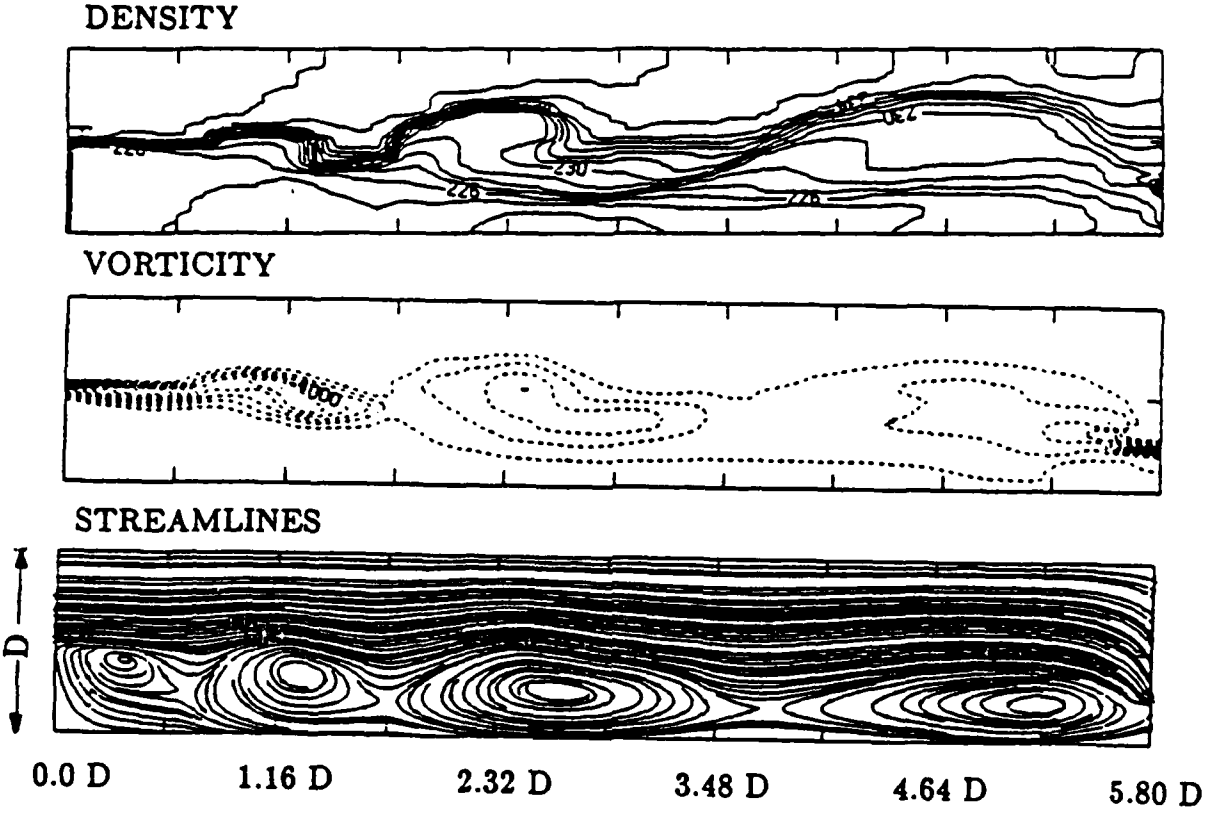

Figure 16. The density, vorticity and streamline contours at timestep 31000 (time = 33.86 ms) from the calculation with acoustic forcing (446 Hz, 0.5% amplitude). Note that only the lower half of the dump chamber is shown and the figure is drawn to scale.

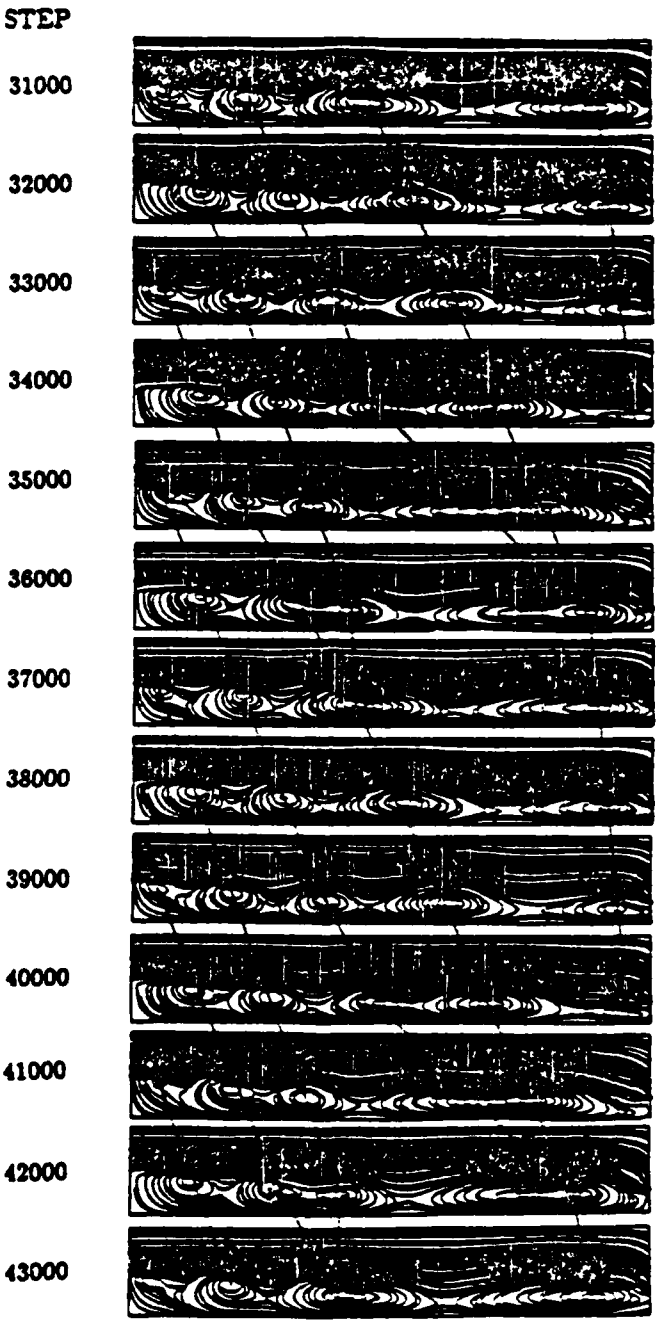

Figure 17. Streamline contours showing the instantaneous flow field in the dump combustor at a sequence of timesteps from calculations on a 40 × 100 grid with acoustic forcing at 446 Hz. The time interval between any two successive frames in the figure is 1.093 ms.

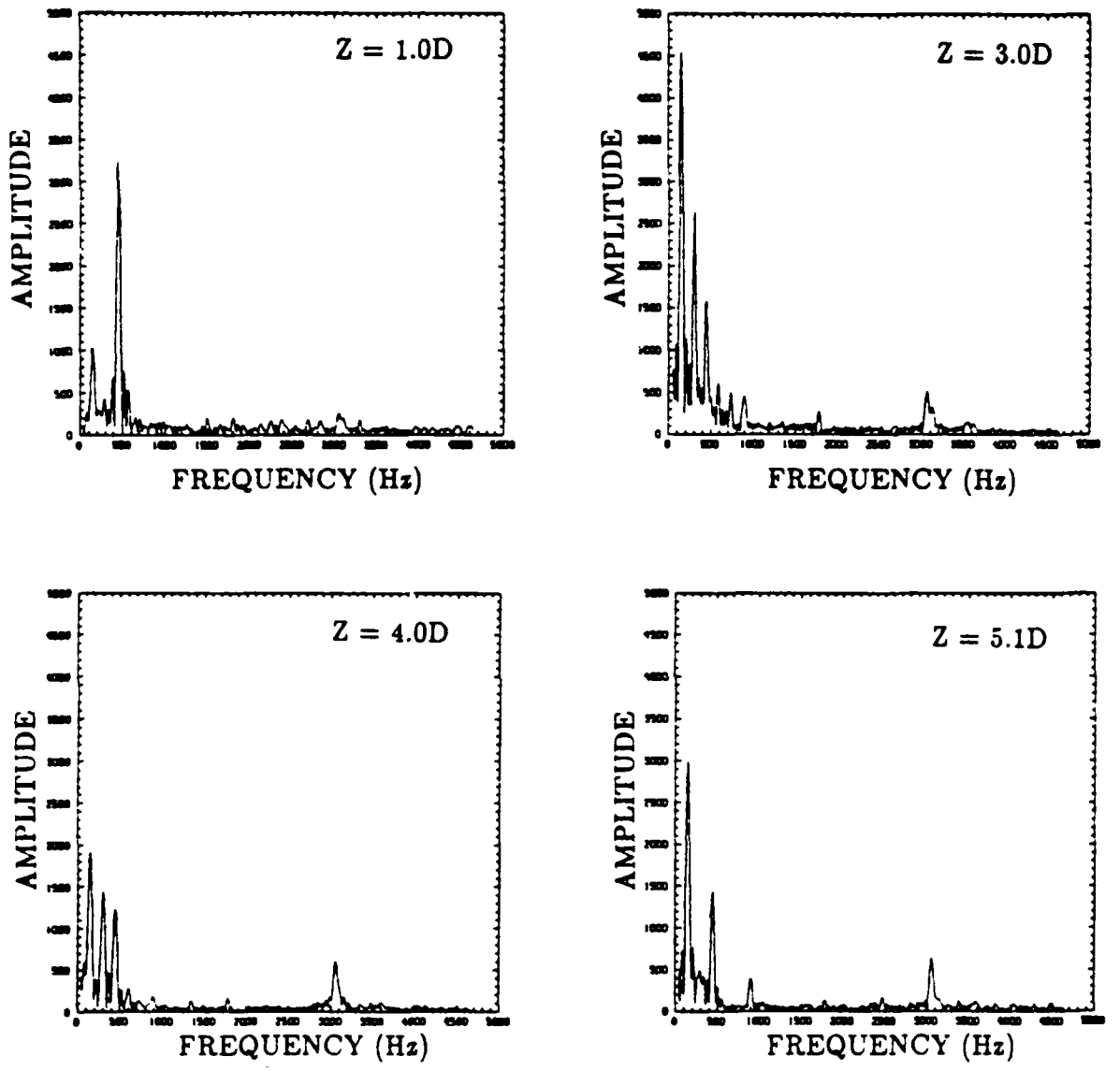

Figure 18. The frequency spectrum of pressure fluctuations at a series of axial positions in the shear layer from the calculation with acoustic forcing (446 Hz, 0.5% amplitude).

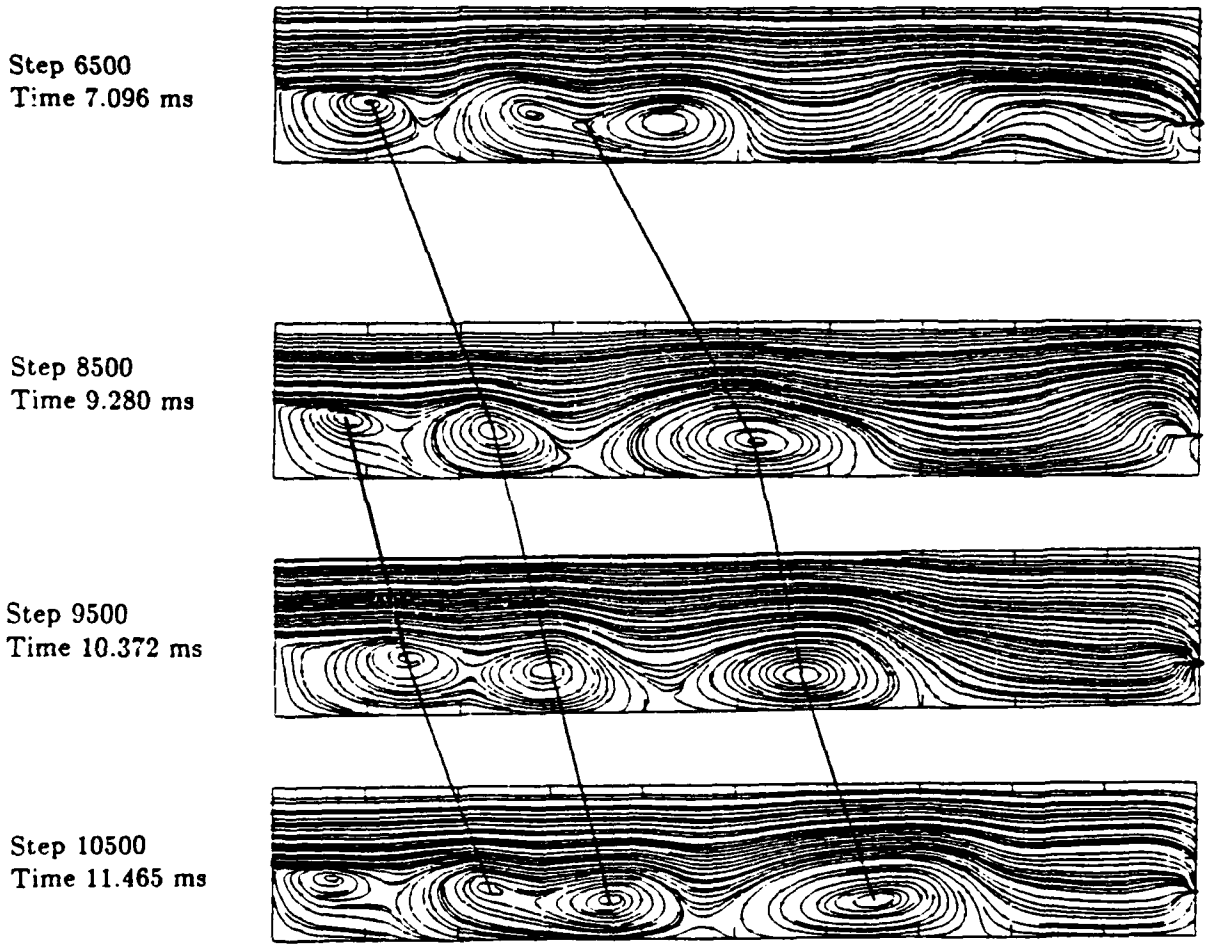

Figure 19. The instantaneous flow field in the dump combustor at four timesteps from the early stages of the calculation on a 40 × 100 grid with acoustic forcing at 446 Hz. Vortex mergings are seen at timesteps 6500 and 10,500 which are 4.37 ms apart giving a frequency of 229 Hz.

REFERENCES

1. Swithenbeck, J., Poll, I., Vincent, M.W., and Wright, D.D., "Combustion Design Fundamentals," *Fourteenth Symposium (International) on Combustion*, The Combustion Institute, Pittsburgh, Pa., 1973, pp. 627-636.

2. Viets, H. and Drewry, J.E., "Quantitative Predictions of Dump Combustor Flowfields," *AIAA Journal*, Vol. 19, April 1981, pp. 484-491.

3. Edelman, R.B., Harsha, P.T., and Schmotolocha, S., "Modeling Techniques for the Analysis of Ramjet Combustion Processes," *AIAA Journal*, Vol. 19, May 1981, pp. 601-609.

4. Scott, J.N., and Hankey, W.L., "Numerical Simulation of Cold Flow in an Axisymmetric Centerbody Combustor," *AIAA Journal*, Vol. 23, May 1985, pp. 641-649.

5. Drummond, J.P., "Numerical Study of a Ramjet Dump Combustor Flowfield," *AIAA Journal*, Vol. 23, April 1985, pp. 604-611.

6. Kailasanath, K., Gardner, J.H., Boris, J.P. and Oran, E.S., "Acoustic-Vortex Interactions in an Idealized Ramjet Combustor," *Proceedings of the 22nd JANNAF Combustion Meeting, Pasadena, CA*, CPIA publication 432, Vol. 1, Oct 1985, pp.341-350.

7. Jou, W.H. and Menon, S., "Numerical Simulation of the Vortex-Acoustic Wave Interaction in a Dump Combustor," AIAA paper No. 86-0002, presented at the AIAA 24th Aerospace Sciences Meeting, January 1986.

8. Schadow, K.C., Wilson, K.J., Crump, J.E., Foster, J.B. and Gutmark, E., "Interaction Between Acoustics and Subsonic Ducted Flow with Dump," AIAA paper No. 84-0530, presented at the AIAA 22nd Aerospace Sciences Meeting, January 1984.

9. Boris, J.P. and Book, D.L., "Solution of Continuity Equations by the Method of Flux Corrected Transport," *Methods of Computational Physics*, Academic Press, New York, 1976, Vol. 16, page 85-129.

10. HO, C.M., and Nosseir, N.S., "Dynamics of an Impinging Jet. Part 1. The Feedback Phenomenon," *J. Fluid Mech*, Vol. 105, 1981,pp. 119-142.